CHAPTER 5

Principles of magnetic resonance imaging – 2

The basic steps for spatial localization of the MR signal were described in Chapter 4. These steps (slice selection, frequency and phase encoding, looping) are common features of nearly all MRI measurements. While the descriptions in Chapter 4 are generally correct as presented, there are additional concepts that are integral to the process and must be considered in order to obtain an accurate understanding of MRI. In most cases, the concepts presented here may be implemented with any of the MRI measurement techniques described in the next chapter.

5.1 Frequency selective excitation

Chapter 2 presented the general concepts of RF excitation and resonance absorption by the protons. The nature of the RF transmitter is described in more detail in Chapter 14, but its basic nature is to amplify or increase the amplitude of an input waveform. MRI scanners manipulate the input RF waveforms via software to achieve the desired output of the transmitter. In principle, the RF transmitter can operate in one of two modes: continuous wave and pulse. Continuous wave (CW) mode operation broadcasts the RF energy at all times. Due to its demands on the transmitter hardware, the output power and frequency range are typically limited. While used in MR scanners historically, CW mode is seldom used in MRI scanners today and will not be discussed further in this book. Pulsed mode operation broadcasts energy for brief periods of time and is the standard operational mode for MRI scanners. The peak power produced by the transmitter is greater than with CW operation, but a wider range of frequencies can be manipulated with greater precision. This increased flexibility is achieved through shaping or crafting the pulse prior to amplification to obtain the desired output.

The RF waveform consists of a set of complex data points with amplitudes and phases that vary with time, typically several hundred in number. These digital points are converted to analog format prior to mixing with the base

MRI Basic Principles and Applications, Fifth Edition.
Brian M. Dale, Mark A. Brown and Richard C. Semelka.

or carrier frequency and amplification. There are several parameters that are used to characterize RF waveforms. Depending on the manufacturer's software, some of these parameters may be accessible to the operator while others may be predefined:

Center frequency. The center frequency of the pulse is normally chosen as the resonant frequency for the particular collection of protons to be excited. For example, this may be a slice for slice selection or spatial presaturation, or fat protons for fat saturation.

Duration. The pulse duration is the length of time that the waveform is broadcast. It is inversely proportional to the bandwidth or range of frequencies that are broadcast by the transmitter; narrower bandwidth pulses require longer RF pulse durations.

Phase. The phase of the pulse defines the effective orientation of the RF energy (see Figure 2.2) and determines the axis of rotation for the net magnetization under the influence of the pulse.

Amplitude. The pulse amplitude, or, more precisely, the pulse amplitude integral, determines the amount of rotation that the protons undergo (flip angle). In addition, the pulse amplitude is related to the amount of energy (power) that the protons absorb and therefore must dissipate through *T1* relaxation.

Nature of synthesizer mixing (modulation). More details of the combination of the RF waveform with the frequency synthesizer are described in Chapter 14. As mentioned previously, the RF pulse waveforms contain a range of frequencies that will be excited by the pulse. There are two methods that are used for merging the waveform with the center frequency produced by the frequency synthesizer:

- Amplitude modulation distributes the energy to all frequencies at the same time during the pulse. This mode ensures that all frequencies are treated equally by the RF transmitter.
- Frequency/phase modulation excites each frequency/phase sequentially during application of the pulse, each at the same amplitude. These pulses frequently are less demanding on the transmitter hardware in terms of peak power output, but require more total power from the transmitter.

Regardless of the type of modulation, most MRI applications require uniform behavior of the frequencies encompassed by the RF pulse by the end of transmission; that is, the RF pulse excites all frequencies equally within its selected range. This translates into a pulse waveform that produces uniform amplitude and phase excitation throughout the frequency range; that is, all affected protons should be rotated the same amount and in the same direction when the transmitter is turned off. This ensures that all protons within the excitation volume will have a common starting point following the excitation process.

Pulse shape. The pulse shape is the mathematical function that best models the waveform in time (the time-domain shape is used as this is the format used as input to the transmitter). There are four shapes that are frequently used:

- *Nonselective* pulses, also known as rectangular or "hard" pulses, are of short duration and constant amplitude and excite a broad frequency range with a uniform amplitude. They are usually used to determine the resonant frequency of the patient or if very short RF pulse durations are required. Nonselective pulses may also be used in a series of pulses applied in a very short time period, known as a composite pulse (see Section 5.2). Strictly speaking, "nonselective" pulses are frequency selective since the pulsed nature of the excitation limits the frequency bandwidth that can be incorporated into the pulse (Figure 5.1).

The remaining pulses are collectively known as frequency selective or "soft" pulses. Frequency-selective pulses do not have a constant amplitude at all times or at all frequencies during broadcasting. Their pulse durations are longer than for a nonselective pulse, allowing for a narrower frequency bandwidth; however, they are still truncated or shortened in time compared to the theoretical pulse shapes, which have infinitely long durations:

- *Sinc* pulses are the primary choice as frequency-selective excitation and refocusing pulses. These pulses provide uniform amplitude and phase excitation throughout the slice. For an RF pulse to excite a particular frequency, that frequency must be included within its bandwidth. As more frequencies at the same phase are included in a pulse, the pulse shape approaches that of a sinc function, an infinite function that contains all possible frequencies in the bandwidth (Figure 5.2). Due to the short duration of the pulse

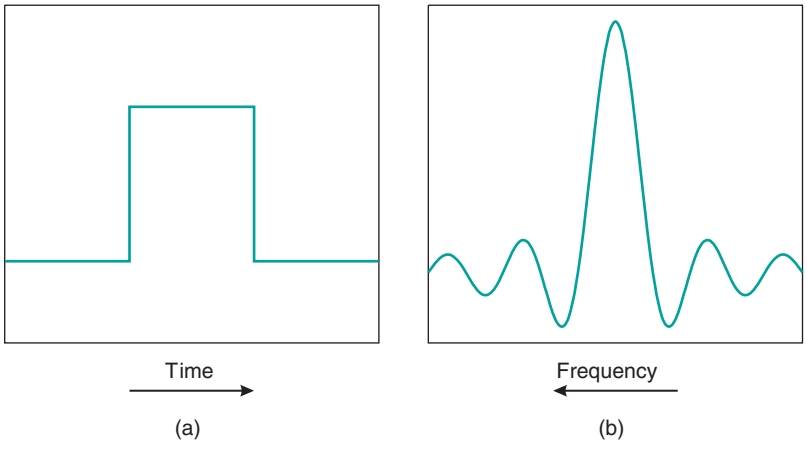

Figure 5.1 Nonselective or rectangular RF pulse: (a) time-domain waveform; (b) frequency-domain waveform.

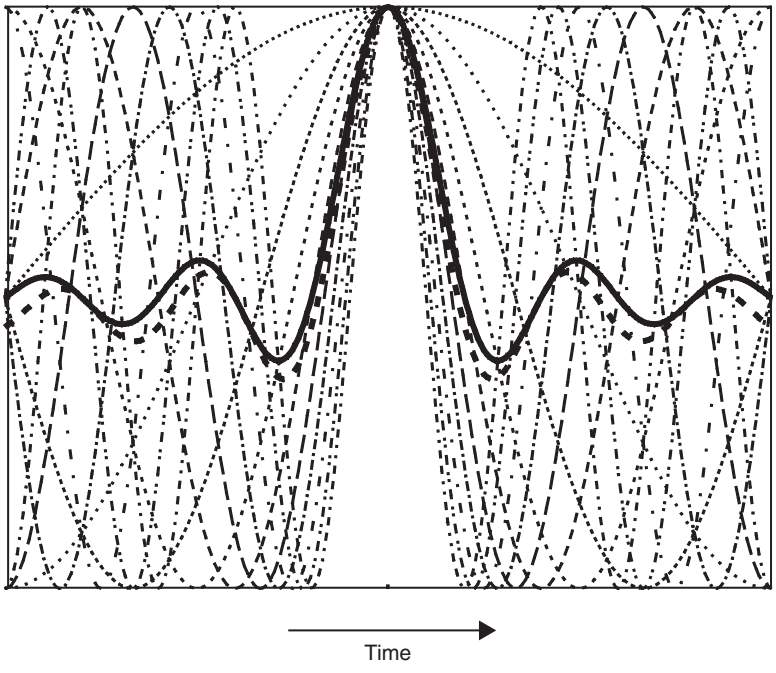

Figure 5.2 A series of sine waves of different frequencies all in phase at one point in time sum to give an approximation (dashed dark line) of an infinite sinc function (solid dark line).

and its limited bandwidth, the actual pulse shape used for slice selective pulses is a truncated sinc function. This truncation causes the frequency cutoff to be less than ideal, with two important consequences: frequencies outside the desired bandwidth are excited as well as those within the bandwidth and the drop-off of the excitation (known as the pulse profile) is not rectangular but has sloped sides. The extraneous excitation can be minimized by filtering the sinc function or mathematically forcing it to zero at the edges. This reduces the total power contained within the pulse, but accentuates the sloped nature of the pulse profile (Figure 5.3).

- *Gaussian* pulses are frequently used for frequency-selective saturation pulses such as fat suppression or magnetization transfer suppression due to a narrower excitation bandwidth (see Chapter 7). These pulses have excitation profiles that follow a Gaussian shape, which is more rounded than the sinc function (Figure 5.4). These pulses are also frequently filtered, which affects the frequency bandwidth.
- *Hyperbolic secant* pulses are often used as inversion pulses in inversion recovery sequences (see Chapter 6). These pulses are applied as phase-modulated adiabatic (literally, "no heat") pulses and produce inversion of the net magnetization with very uniform frequency profiles independent of transmitter amplitude levels. Hyperbolic secant pulses have phase variations that make them unsuitable for use as a refocusing pulse (Figure 5.5). They also generally have higher power deposition that either sinc or Gaussian pulses.

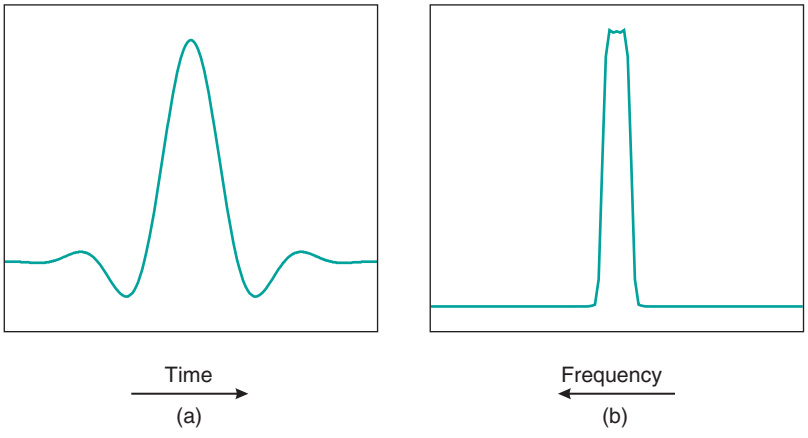

Figure 5.3 Truncated sinc RF pulse: (a) time-domain waveform; (b) frequency-domain waveform.

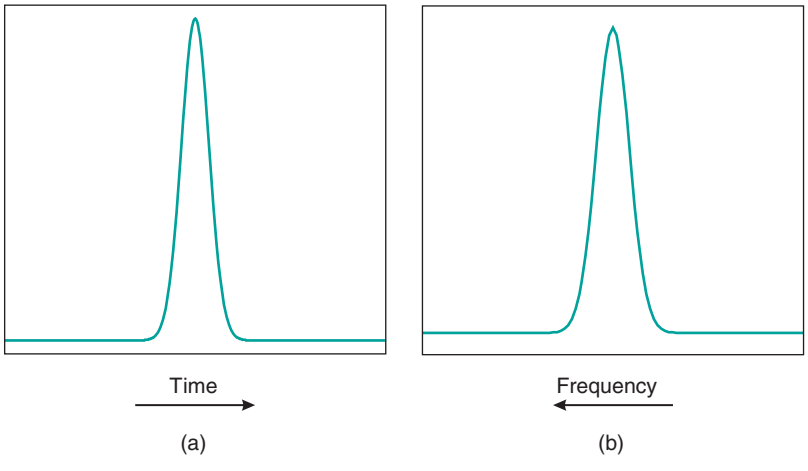

Figure 5.4 Gaussian RF pulse: (a) time-domain waveform; (b) frequency-domain waveform.

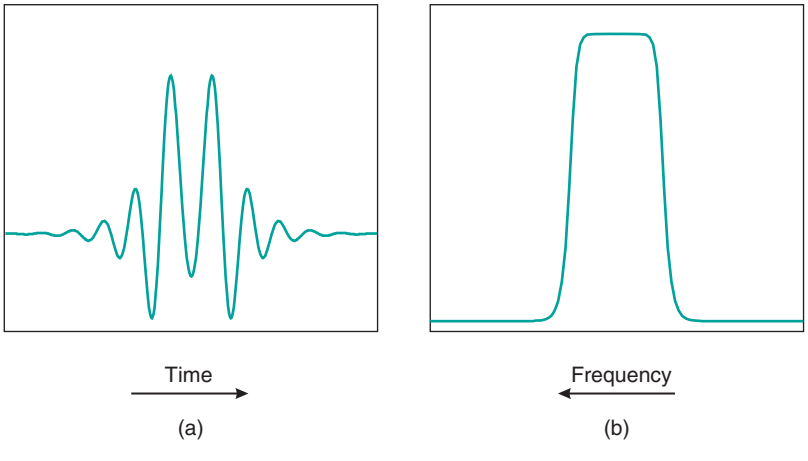

Figure 5.5 Hyperbolic secant or adiabatic RF pulse: (a) time-domain waveform; (b) frequency-domain waveform.

In general, RF excitation pulses are subject to several competing criteria:

1. Short duration pulses require high peak pulse amplitudes to achieve the same pulse area (flip angle). Depending on the particular RF amplifier and transmitter coil, the maximum power that can be broadcast is limited.
2. As the pulse amplitude increases, the power deposited by the pulse also increases in a quadratic fashion (a factor of two increase in the pulse amplitude causes a factor of four in the pulse power). This fact may require longer pulse durations to minimize RF power deposition, which may require an increase in *TE* and *TR*.
3. Sinc functions produce rectangular, phase coherent excitation profiles only with low flip angles (<30°). High amplitude sinc pulses such as 90° or 180° pulses have excitation profiles that are significantly nonrectangular. Manufacturers strive to provide uniform excitation profiles, subject to the other criteria. Specific questions about particular RF pulse profiles should be addressed to the individual manufacturer.
4. As the RF pulse duration increases, the bandwidth of the pulse decreases. This means that less G_{SS} is required to focus the energy to the same tissue volume. However, as G_{SS} is reduced, the sharpness of the slice profile (known as the transition region) is reduced as well. This can cause more pronounced crosstalk between slices or sensitivity to magnetic susceptibility differences within the slice, producing nonuniform image intensities, particularly at ultra-high field strengths.

5.2 Composite pulses

The RF pulses described above are typically applied as a single unit; that is, the manipulations of the spin are performed by a single waveform that is broadcast at the appropriate time. A composite RF pulse is a series of closely spaced RF pulses applied over a short time period that together affect the protons like a single pulse. The pulse amplitudes for each RF pulse typically form a binomial progression (e.g., 11, 121, 1331), with the effective flip angle being the sum of the individual flip angles. The timing between the pulses allows protons with different resonant frequencies to cycle in phase and undergo different effects from each pulse (Figure 5.6). The individual pulses may be nonselective (rectangular) or frequency selective, resulting in a composite pulse of the same character. In general, composite pulses require less transmitter power than single RF pulses for the same flip angle because of the short duration of the individual pulses. However, the total time required for the combined excitation is longer than for a single excitation pulse. Composite pulses can be used for general slice excitation, but the most common application is for signal suppression (see Chapter 8).

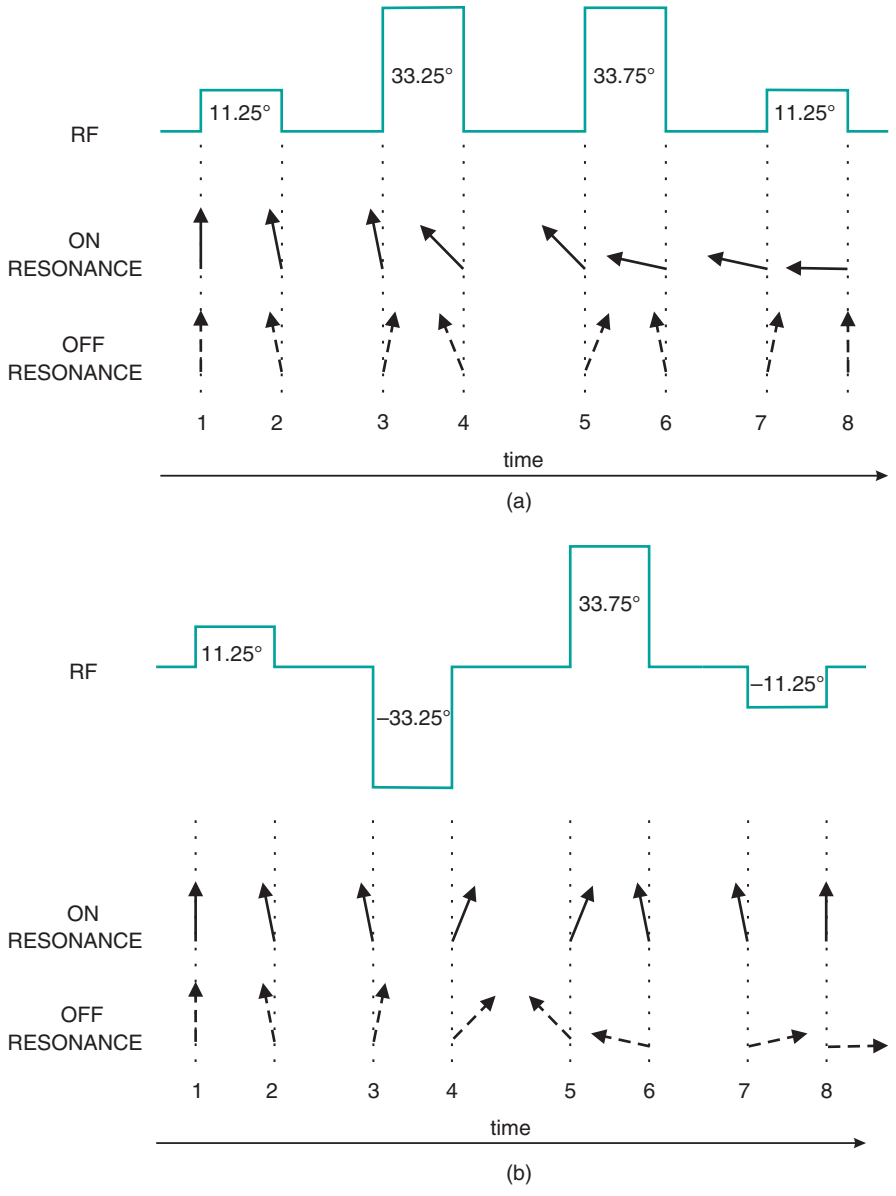

Figure 5.6 Composite pulses. (a) A 1331 composite pulse is shown with a total excitation angle of 90°. A rotating frame corresponding to the on-resonant frequency is assumed. Prior to the first RF pulse (1), both on-resonance (solid arrow) and off-resonance (dashed arrow) protons are unexcited. At the end of the first RF pulse (2), both will be excited 11.25°. Because of the difference in resonant frequencies, the off-resonance protons become out of phase. The time for the second RF pulse (3) is chosen so that the off-resonance protons are exactly 180°out of phase. At the end of the second RF pulse (4), the on-resonance protons are excited 45°while the on-resonance protons are excited 22.5°. The delay between the second and third RF pulses is chosen so that the off-resonance protons are 180°out of phase with the on-resonance proton (5). A similar delay is chosen between the third and fourth RF pulses (6,7). At the end of the fourth RF pulse (8), the on-resonance protons are rotated 90°(excited), while the off-resonance protons are at 0°(unexcited). (b) A 1331 composite pulse with a total excitation angle of 90°. The end result differs from (a) in that the on-resonance spins are not excited while the off-resonance spins are rotated 90°.

5.3 Raw data and image data matrices

In analyzing measured MRI data, two formats for the data may be used: raw data and image data. Both data sets contain the same information from the slice or slices and both formats are used for different purposes. They are stored and manipulated as a grid or matrix of points representing the slice. The two formats are related by the Fourier transformation, with the raw data being the format generated by and used in the data collection process and the image data being the format normally used for viewing and interpretation.

In MRI, the raw data consists of the digitized data measured for a given echo from a given slice or volume of tissue. Whether an analog or digital receiver is used (see Chapter 14), the echo signal amplitude measured by the receiver coil is digitized as a function of time. The amplitude variations have a shape roughly corresponding to a sinc function (see Figure 5.2). The digital form of the signal is stored as a complex data array with each signal point represented by real and imaginary values. For the raw data matrix, the detected signal amplitudes for a given echo correspond to a row and each row differs by the value of G_{PE} applied prior to detection. The rows are typically displayed in order of increasing phase encoding amplitudes from top to bottom, corresponding to maximum negative to maximum positive G_{PE} amplitudes, respectively. The raw data matrix is thus a grid of points with the readout direction displayed in the horizontal direction and the phase encoding direction displayed in the vertical direction. Its dimensions depend on the number of readout data points and the number of phase encoding steps for the scan (Figure 5.7).

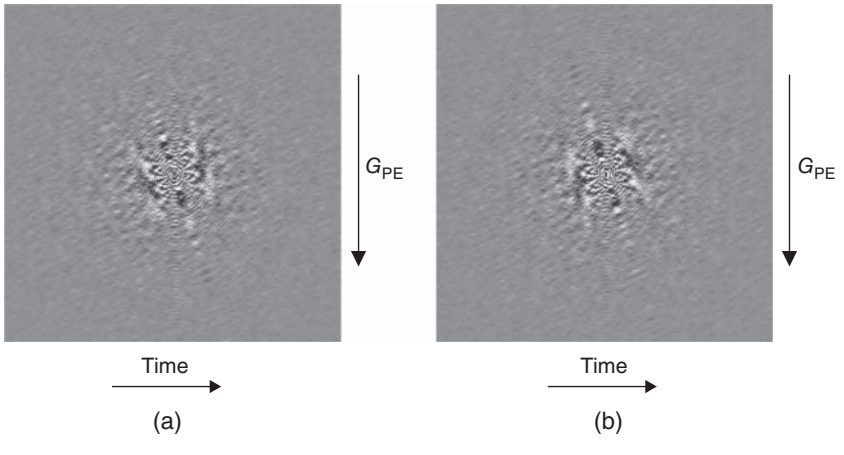

Figure 5.7 Raw data, real (a) and imaginary (b). The raw data matrix has dimensions of $N_{PE} \times N_{RO}$. Each row is a measured signal at a particular $\boldsymbol{G_{PE}}$. The number of rows corresponds to N_{PE}. Signals acquired with high negative amplitude $\boldsymbol{G_{PE}}$ are displayed at the top, low amplitude G_{PE} in the middle, and high positive amplitude G_{PE} at the bottom of the matrix. Each column corresponds to a data point sampled at a different time following the excitation pulse.

The image data or display matrix is obtained via the 2D Fourier transformation (rows and columns) of the complex raw data matrix. The image matrix is a

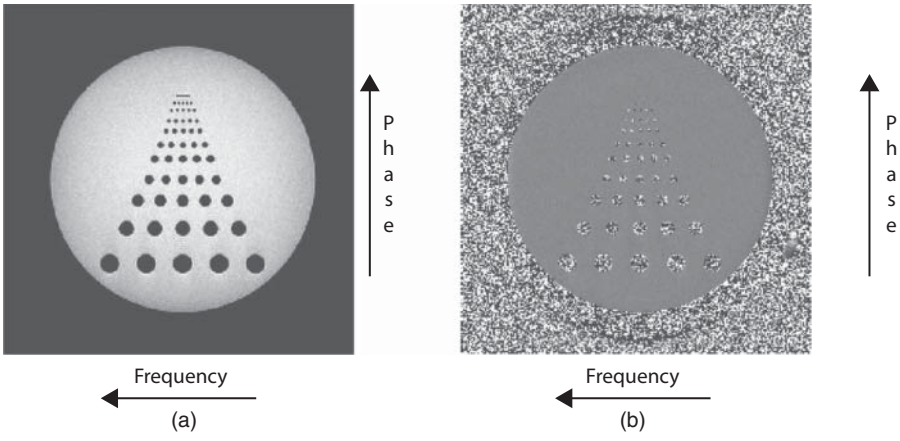

Figure 5.8 Image data, magnitude (a) and phase (b). The image data is obtained by performing a two-dimensional Fourier transformation on the data set displayed in Figure 5.7. The rows and columns correspond to the phase-encoding and readout directions. The specification of rows and columns as readout and phase-encoding directions is usually set by the operator.

complex frequency and phase map of the proton signal intensity from a volume element weighted by the *T1* and *T2* values of the tissues contained within the volume. The specific frequencies and phases are unique to the location of the volume element and are measured relative to the base transmitter frequency. Rather than viewing images as complex arrays, the displayed image matrix is normally an array of real or integer values, consisting either of the signal magnitudes or the relative phases at each point. Although they must be the same dimension as the raw data matrix, image matrices are usually displayed as square arrays with readout as one direction and phase encoding as the other direction in the image (Figure 5.8). To accomplish this, a process known as interpolation may be performed in which additional image pixels are created by the Fourier transformation process that are derived from the original pixels. For example, if a 192 PE × 256 RO matrix is acquired, the image that results is 256 rows × 256 columns, with 64 "extra" pixels created in the PE direction by the Fourier transformation. The choice of rows and columns for readout and phase encoding is at the operator's discretion and is normally made to minimize artifacts in the area of interest. The maximum dimensions in the displayed image matrix normally correspond to the chosen FOV in each direction.

5.4 Signal-to-noise ratio and tradeoffs

One of the most important characteristics of both the raw data and image data is the signal-to-noise ratio (SNR). The SNR of MRI data depends on both the level of signal and the level of noise present in the data, each of which depends on many factors. A

voxel with a larger volume contains more signal, and therefore has a higher SNR. Longer sampling time reduces the noise, and therefore increases the SNR. In addition, the MRI hardware contributes to the SNR through the main magnetic field strength, the receive coil sensitivity and volume, and the receive chain noise performance characteristics. Finally, the tissue itself contributes to the signal as determined by its relaxation and other characteristics that affect the specific pulse sequence being used. These effects can be stated as follows:

$$SNR = V * T^{1/2} * R(B0, B1, \ldots) * I_{seq}(T1, T2, TE, TR, \ldots) \quad (5.1)$$

where V is the voxel volume, T is the total sampling time for each voxel, R is a factor characterizing the SNR of the hardware and processing chain including the main magnetic field, the receive coil sensitivity, and so forth, and I_{seq} is a factor characterizing the signal intensity from the pulse sequence and the tissue.

In equation (5.1) the factor R is generally considered fixed since alterations to R usually require the purchase of a new MRI system or new MRI receive coils. Similarly, I_{seq} is fixed in the sense that it contains the information that is desired from the MRI exam. It is the interaction of the pulse sequence with the tissue that emphasizes the tissue characteristics in the measured signal, so changes to I_{seq} would change the diagnostic information in the image.

This leaves V and T as the only free parameters that can be varied as needed for a given patient in order to improve SNR. Equation (5.1) shows that the SNR is proportional to the voxel volume and the square root of the sampling time. This represents the fundamental compromise, or tradeoff, of MR imaging. If an improvement in the SNR is required, then either spatial resolution or sampling time must be sacrificed. If an improvement in spatial resolution is required, then either SNR will be reduced or sampling time will be increased, etc.

5.5 Raw data and *k*-space

The raw data matrix is a significant concept in MRI. Prior to data processing, each slice will be represented by a raw data matrix. All the information necessary to reconstruct an image is contained within the raw data matrix. Each data point contributes to all aspects (frequency, phase, and amplitude) of every location within the slice, though some data points emphasize different features in the final image. The maximum signal content is located in the central portion of the raw data matrix. These lines are acquired with low amplitude G_{PE} and the measured signal amplitude variations are predominantly due to differences in the inherent tissue signals. These lines are primarily responsible for the contrast in the image. The outer portions of the raw data matrix have relatively low signal amplitude and are acquired with either high positive amplitude or high negative

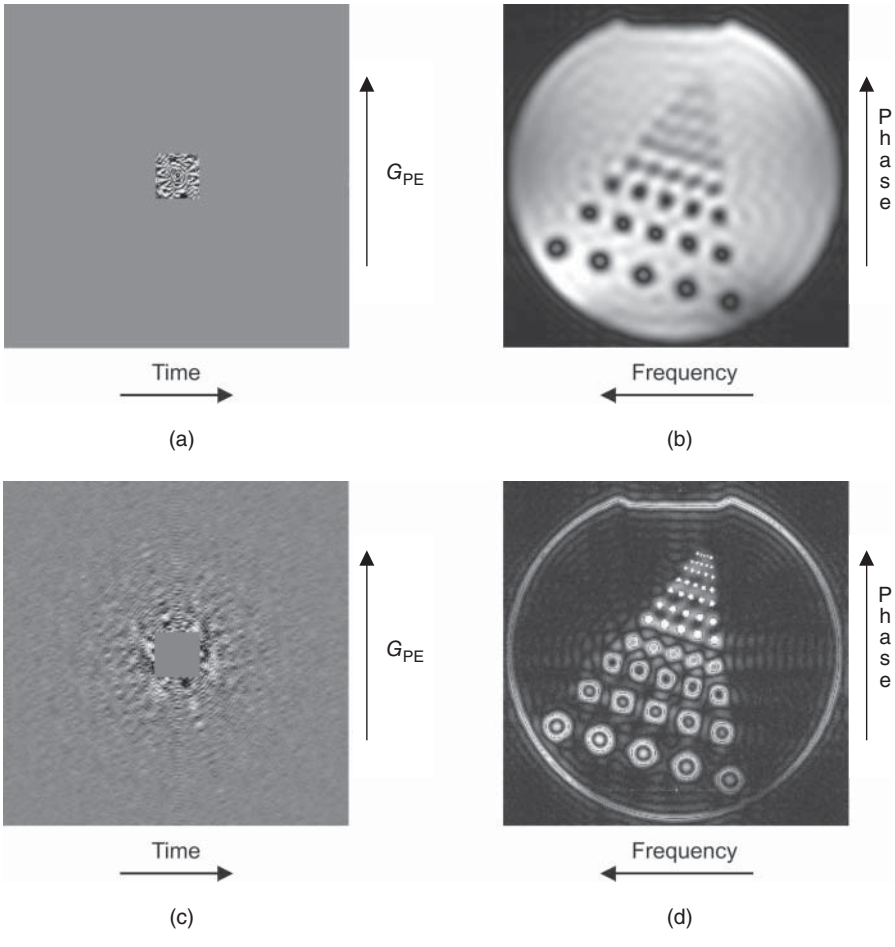

Figure 5.9 Raw data and corresponding images. (a) Same raw data set as Figure 5.7 except that only the central 32 × 32 data points are kept and zero values are defined for the remaining data. Imaginary portion not shown. (b) Magnitude image data of (a). The image intensity is approximately the same as that of Figure 5.8a, but there is a loss of edge definition, exhibited as blurring in the phantom. (c) Same raw data set as Figure 5.7 except that the central 32 × 32 data points are eliminated, corresponding to 1.56% of the total data set. Imaginary portion not shown. (d) Magnitude image data of (c). The image intensity (central portion of the phantom) is virtually absent, while the edges of the phantom are present.

amplitude G_{PE}. These gradients produce high frequencies (by the Larmor equation) and provide mainly edge definition to the resultant image (Figure 5.9).

An alternate method to describe the raw data matrix is called the *k*-space formalism. It provides a convenient way to describe methods for acquiring raw data. In this approach, the complex array of raw data points is treated as a two-dimensional grid of points (k_x, k_y). Each k_x value corresponds to a point in the readout direction of the raw data

matrix and each k_y value corresponds to a point in the phase encoding direction of the raw data matrix. Each (k_x, k_y) data point corresponds to the echo signal amplitude influenced by the combination of readout and phase encoding gradient areas or moments (time * gradient amplitude):

$$k_x = \gamma G_{RO} t_{RO}$$
$$k_y = \gamma G_{PE} t_{PE} \quad (5.2)$$

where t_{RO}, t_{PE} corresponds to the cumulative time that the respective gradient is active. The total gradient influence at each (k_x, k_y) point in the matrix is different and unique. The point (0, 0), referred to as the origin of *k*-space, has the maximum amplitude in the raw data matrix ($G_{PE} = 0$, maximum data point of the echo signal). The *k* values are measured in units of mm^{-1} and are often referred to as spatial frequencies, in analogy with cyclical frequencies measured in units of s^{-1}. The change in *k* in each direction from point to point (Δk_x or Δk_y) is inversely related to the FOV in that direction. Using *k*-space terminology, contrast in the image is primarily determined by low spatial frequency data near the center while edge definition is primarily determined by high spatial frequency data at the edges of *k*-space.

For 3D volume scanning, the *k*-space description requires the addition of a third dimension, k_z, corresponding to the partitions gradient mentioned in Chapter 4:

$$k_z = \gamma G_{SS} t_{SS} \quad (5.3)$$

where t_{SS} is the cumulative time that the slice selection gradient G_{SS} is active. In general, the principles discussed above for *k*-space of two-dimensional images are also true for 3D volume scanning. The raw data space is a three-dimensional volume defined with three coordinates (k_x, k_y, k_z), analogous to the two-dimensional volume defined by (k_x, k_y) described earlier. The change in k_z from step to step (Δk_z) controls the distance of accurate measurement in the slice direction (typically matching the volume of RF excitation). The origin of the volume (0, 0, 0) contributes most to the contrast and the edges of the *k* volume contribute edge definition in the resulting images. The 3D looping structures illustrated in Figure 4.11 can be identified as the two ordering schemes for varying the k_y and k_z gradient amplitudes, either fixed k_z-varying k_y or fixed k_y-varying k_z, respectively.

Two requirements to produce artifact-free images are for the raw data space to be sampled continuously (no gaps in lines or columns) and with a uniform density in a given direction. In terms of *k*-space, Δk_x and Δk_y must be constant but not necessarily equal and must span the entire space. This requirement ensures equal weight to both contrast and edge definition in the final image. One approach to accomplish these requirements, used in traditional scanning, involves a rectilinear data collection. Each MR signal is measured in the presence of a constant amplitude G_{RO} with the same number of sample points measured at a constant rate (constant dwell time). The phase encoding gradient G_{PE} is changed by a constant increment (ΔG_{PE}) from line to line (Figure 5.10). When a complete set of G_{PE} lines is acquired, a raw data set is produced that fulfills both criteria.

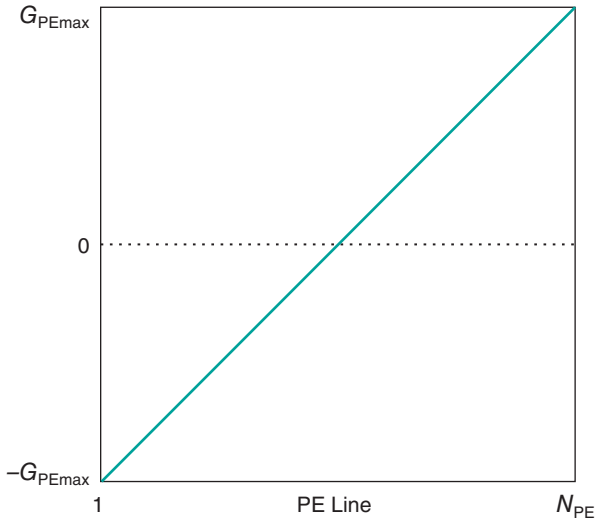

Figure 5.10 Sequential k-space filling. Each line of k-space (phase-encoding line) corresponds to a measured MR signal. Lines of k-space are acquired serially in time with the data from the maximum negative G_{PE} acquired first and the data from the maximum positive G_{PE} acquired last. The center of *k*-space ($G_{PE} = 0$ mT m^{-1}) step is acquired halfway through the data collection period. This is the traditional data collection method.

5.6 Reduced *k*-space techniques

The requirements for continuity and uniform density of the raw data matrix do not require that a complete raw data be measured in order to produce artifact-free images. Since many MRI scans are several minutes in duration, methods to reduce the scan time while maintaining image fidelity are desirable. Since the scan time is proportional to the number of phase encoding steps N_{PE}, a common approach to reduce the scan time is to reduce the number of measured G_{PE} amplitudes. If the measured amplitudes are properly chosen, then the above-mentioned requirements can be fulfilled. Two approaches reduce the total number of G_{PE} amplitudes symmetrically around $G_{PE} = 0$. One method keeps the change in amplitude ΔG_{PE} between successive steps (or, equivalently, Δk_y) equal to that for the "complete" raw data matrix, so that the FOV in the phase encoding direction is the same in both images. The maximum G_{PE} values are smaller than those for the complete raw data matrix. The missing lines are replaced by zeros prior to Fourier transformation, a process known as zero-filling, so that the final image matrix is square, as described in Section 5.2. This results in a loss of spatial resolution in the final image due to the loss of information at high spatial frequencies (Figure 5.11). The other method increases ΔG_{PE} (Δk_y) so that the maximum G_{PE} values are equal to the complete raw data matrix. In this case, the FOV in the phase encoding direction is reduced, regaining the loss in spatial resolution due to the reduced number of lines. However, the spatial region of accurate phase measurement is reduced, potentially causing aliasing artifacts. These may be detrimental to the image quality (see Chapter 9) or used

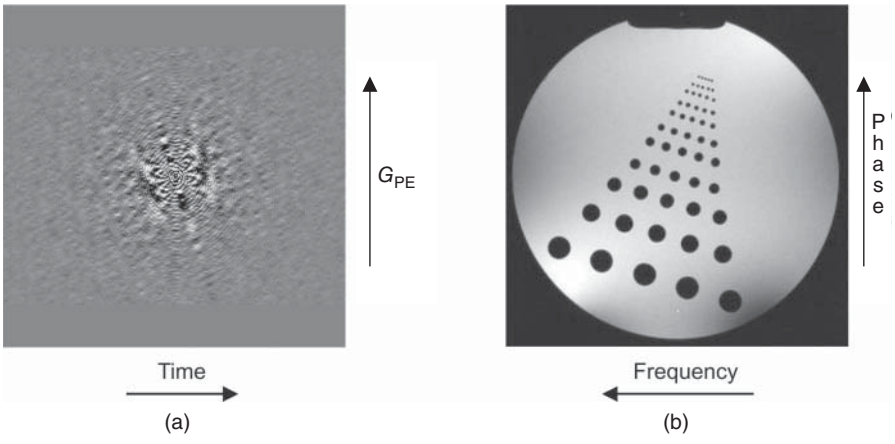

Figure 5.11 Raw data and corresponding image. (a) Raw data set for 192 lines measured with the same ΔG_{PE} as for Figure 5.7, and zero values are defined for the remaining data. Imaginary portion not shown. (b) Magnitude image data of (a). The FOV is identical and the image intensity is almost identical to that of Figure 5.8a, but there is a slight loss of edge definition, exhibited as blurring in the phantom.

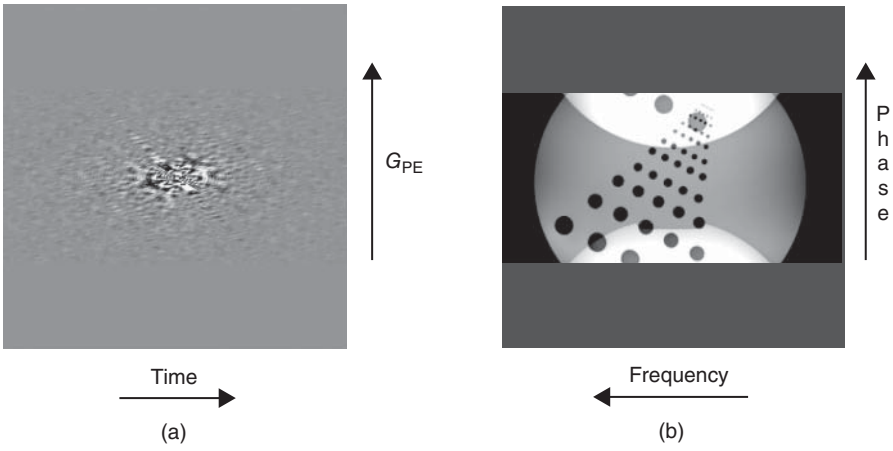

Figure 5.12 Raw data and corresponding image. (a) Raw data set for 192 lines measured with an increased ΔG_{PE} compared to Figure 5.7, and zero values are defined for the remaining data. Imaginary portion not shown. (b) Magnitude image data of (a). The FOV is reduced compared to that of Figure 5.8a, causing aliasing artifact. (a) (b) GPE

as part of the data collection process (see Section 5.10). In addition, the final image is often padded with extra lines to make the final image display square, which reduces the portion of the total image that contains useful information (Figure 5.12). Use of a reduced number of G_{PE} lines (e.g., 192 PE lines $\times$ 256 RO points) also fulfills the requirement for a "continuous" *k*-space, since the "missing" lines are at the edges of *k*-space and that there are no gaps in the interior.

A third method for reducing the number of measured raw data lines is known as partial Fourier imaging. Due to the usage of positive and negative polarity G_{PE} gradients, a symmetry to the raw data matrix is generated. This symmetry is known as Hermitian symmetry, with the negative amplitude gradients producing real signals with the same amplitude and opposite phases as the signals generated by the positive amplitude gradients (Figure 5.13). The partial Fourier technique reduces the total number of lines acquired for the raw data matrix, but in an asymmetric fashion about the $G_{PE} = 0$ line. The maximum amplitude G_{PE} and ΔG_{PE} between each acquisition are the same as for a complete raw data matrix, maintaining the spatial resolution and FOV, respectively. The missing raw data (high positive amplitude G_{PE}) are extrapolated from the measured data through the Hermitian symmetry prior to Fourier transformation. The resulting image has the same FOV and spatial resolution as that from a complete raw data matrix, but the scan time is reduced. The problems with partial Fourier techniques are a loss in SNR due to the reduced number of measured lines (reduced T in equation (5.1)) and an enhanced sensitivity to artifacts due to the artificial replication of the information; in effect, an artifactual signal is duplicated rather than being averaged.

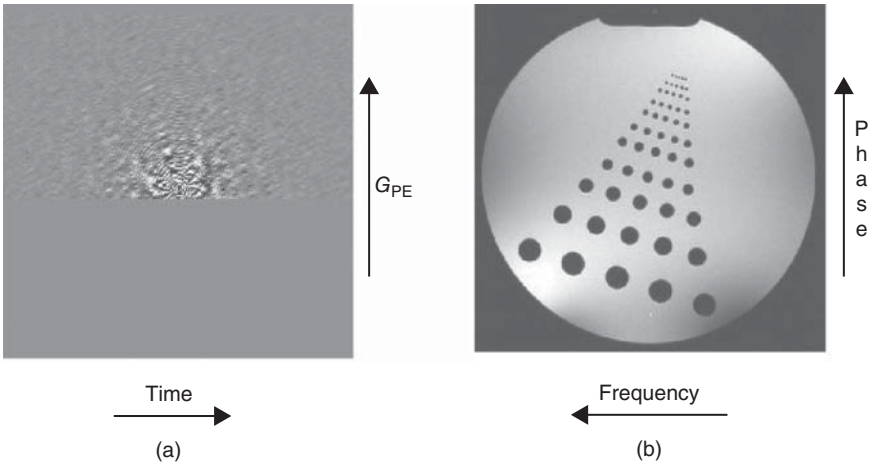

Figure 5.13 Raw data and corresponding image. (a) Same raw data set as Figure 5.7 except that only the upper 136 lines are kept, and zero values are defined for the remaining data. Imaginary portion not shown. (b) Magnitude image data of (a). The spatial resolution and signal intensity are identical to those of Figure 5.8a, but there is a slight increase in noise.

Reduction of data in the readout direction is also possible; however, the scan time is not directly affected. These methods typically involve reducing the number of sample points for the echo while maintaining G_{RO} and the dwell time. This allows a shorter total sampling time to be used, reducing the sequence kernel time and allowing a shorter minimum *TR* to be used or more slices to be measured. This reduced sampling can be performed symmetrically with zero-filling or, asymmetrically, producing a half-echo. In this case, as in the case of a partial Fourier in the PE direction, the missing data are extrapolated based on the Hermitian symmetry of the echo.

5.7 Reordered *k*-space filling techniques

While a complete *k*-space of uniform density is necessary prior to Fourier transformation, the order in which the individual k_y lines are acquired is somewhat arbitrary. This filling order is also known as the *k*-space trajectory. The traditional method for data collection is sequential filling or a linear trajectory. The raw data matrix is filled, one line at a time, with adjacent k_y lines acquired serially in time. The readout gradient G_{RO} is applied for a constant period of time and amplitude, during which time the echo is sampled with a constant dwell time. Depending on the particular manufacturer and pulse sequence, the scan may begin with the most negative G_{PE} and end with the most positive G_{PE} (increasing amplitudes) or the opposite (decreasing amplitudes). In either case, G_{PE} is varied in a linear fashion and the $k_y = 0$ signal is measured halfway through the data collection (see Figure 5.10).

Other methods for filling *k*-space are used for special applications or when additional contrast control is required. Reordered *k*-space refers to methods of data collection where the raw data are acquired in a nonsequential fashion. Centric ordering acquires the low amplitude G_{PE} steps earliest in the scan, with higher amplitude G_{PE} steps acquired later (Figure 5.14). Variations on sequential and centric ordering are possible, in which the $k_y = 0$ signal is acquired at other times of the scan. These approaches may be useful in scans where the net magnetization ***M*** is not sufficiently close to a steady-state value in the initial detected echoes. Acquiring the $k_y = 0$ signal at a time shortly after the scan begins will allow ***M*** to reach a value closer to the steady-state value using the initial RF excitation pulses of the sequence rather than "dummy" excitation pulses.

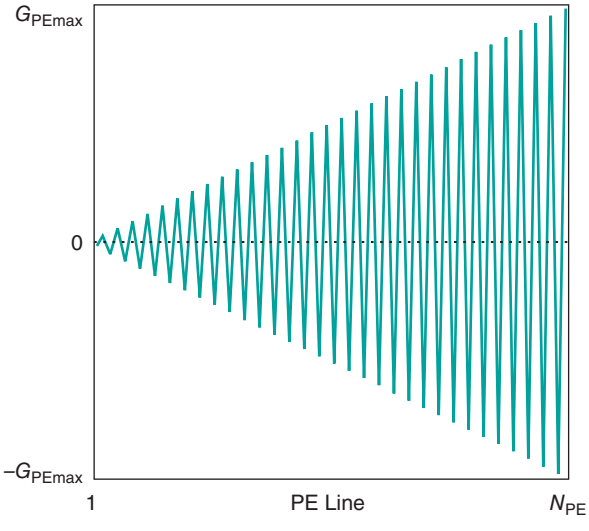

Figure 5.14 Centric *k*-space filling. Lines of *k*-space are acquired serially beginning at the center of *k*-space, then in increasing $\boldsymbol{G}_{PE}$ amplitudes of alternating polarity.

Another useful approach for data collection is the segmented method, in which successive echoes in the scan measure lines from different regions or segments of *k*-space. Data are collected in a segment-serial fashion, one phase encoding step from each segment. The number of segments, the number of lines per segment, and the order of acquisition may be independently varied (Figure 5.15), though the total number of measured lines will be the product of the number of lines per segment times the number of segments.

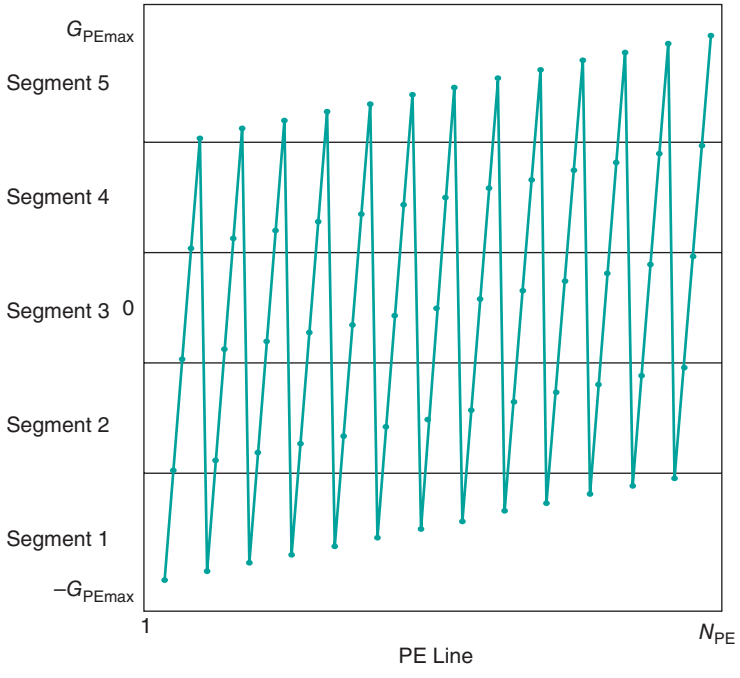

Figure 5.15 Segmented *k*-space filling. Lines of *k*-space are acquired in groups or segments. The example here shows five segments. One line of data is acquired from each segment before a second line is acquired from any segment. The center of *k*-space is acquired at a time during the scan that is dependent on the number of lines per segment, number of segments, and the order of acquisition within a segment and between segments.

For 3D scanning, the reordering of *k*-space can be done in different ways. The two gradient tables (k_y and k_z) are independent of each other and need not be varied in the same fashion. For example, one table may be sequential stepping while the other may be centric or segmented. Spiral scanning in 3D refers to the stepping order of the $k_y - k_z$ gradients in which the two amplitude variations form a spiral (Figure 5.16). This approach is useful in acquiring the contrast-determining echoes early in the measurement, allowing control of tissue contrast, or minimizing motion artifacts.

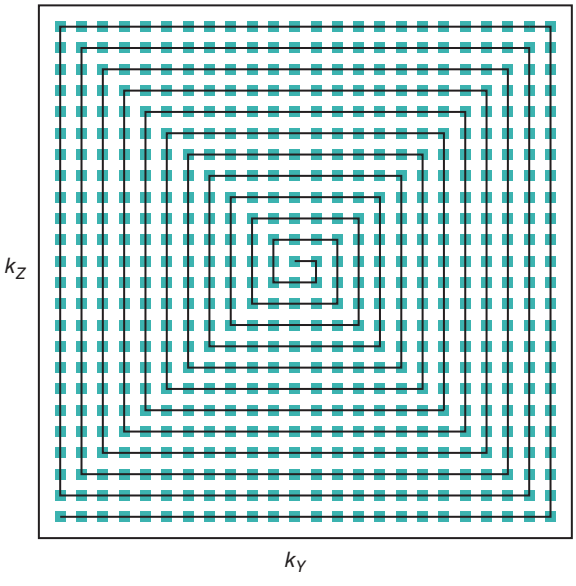

Figure 5.16 Spiral filling of *k*-space, three-dimensional. The k_y and k_z amplitudes are varied in an increasing spiral pattern. The lowest-amplitude values are used to acquire the earliest echoes in the scan.

5.8 Other *k*-space filling techniques

As mentioned in Section 5.3, a continuous (gap-free) raw data set of uniform density must be acquired prior to Fourier transformation to minimize image artifacts. This may be accomplished in several ways. Conventional scan techniques sample the echo signal with a constant dwell time and a constant G_{RO} and use a G_{PE} that varies with constant increment. This is the easiest approach to ensure a constant Δk_x and Δk_y. Nonrectilinear sampling occurs when either of these conditions is not fulfilled. Three important examples of this are ramped sampling, spiral sampling, and radial sampling.

Ramped sampling is a simple variation from the traditional rectilinear sampling. A normal gradient pulse consists of two amplitude-varying parts known as the ramps (a ramp up and a ramp down) and a constant amplitude portion known as the plateau or flat-top (see Chapter 6). If sampling of the echo occurs while G_{RO} is changing (sampling during the ramp time), the effect of G_{RO} will not be uniform for each sample point of the echo (Δk_x will not be constant) (Figure 5.17). Ramped sampling may be desired in order to obtain specific measurement parameters (for instance, a shorter *TE*). The problem of variable Δk_x when performing ramped sampling can be eliminated either by using variable dwell time sampling, ensuring that Δk_x is constant during sampling, or by

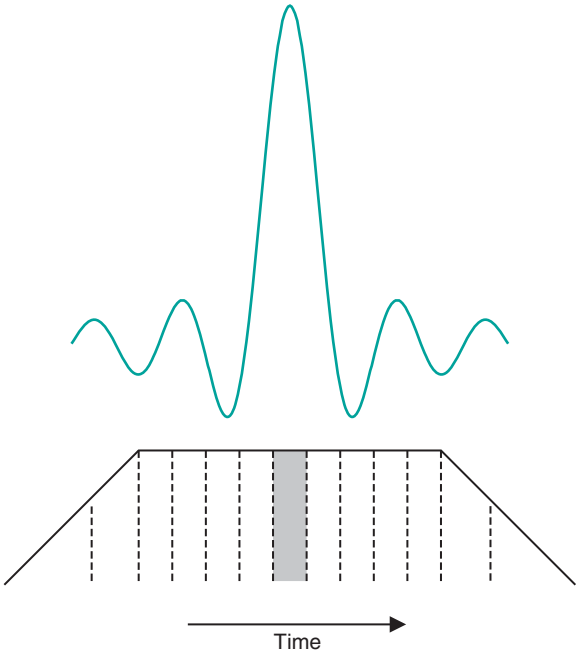

Figure 5.17 Ramped sampling of signal. The dashed lines represent the time points when signal sampling occurs. The $\boldsymbol{G_{RO}}$ gradient amplitude is not constant during signal sampling. As a result, Δk_x, which is proportional to the rectangular gray area, is not constant for all sample points.

performing a regridding of the measured data prior to Fourier transformation. Regridding creates a constant Δk_x from the measured data using interpolation methods to generate the missing data points. The computational difficulty of the regridding method depends on the nature of the G_{RO} variation. Ramped sampling is similar to conventional sampling in that the readout process (G_{RO} and sampling rate) are identical for all echoes used to generate the image.

The other approaches have G_{RO} values that differ from echo to echo. One method is known as projection reconstruction, frequently implemented as radial scanning. Projection reconstruction uses a constant G_{RO} but its direction changes from echo to echo. The two gradients that are perpendicular to G_{SS} are combined with different ratios, which generate different perspectives or projections of the slice. Each digitized signal produces a line of raw data, but the lines are in different directions (Figure 5.18). One advantage of radial scanning is that each echo samples the center of *k*-space, so that each signal will have an equivalent SNR. The primary disadvantage is that the sampling density of *k*-space will not be uniform (the points near the center of *k*-space (Δk_x, $\Delta k_y \approx 0$) are sampled more densely than those near the edges of *k*-space). Also, Δk_x and Δk_y will normally not be constant. As a result, a regridding of the raw data must be performed prior to Fourier transformation in order to produce images without phase artifacts. In addition,

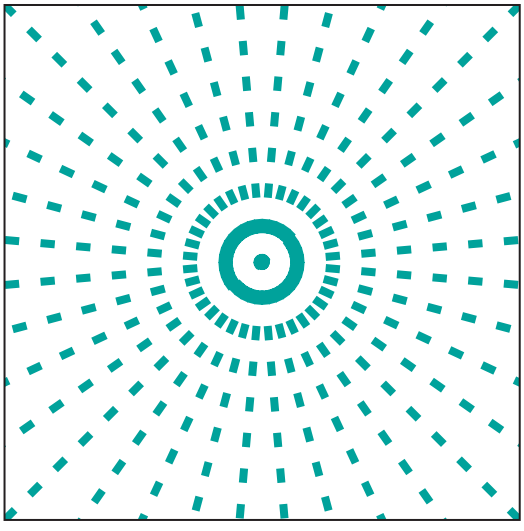

Figure 5.18 Radial filling of *k*-space. Each signal is sampled with a $\boldsymbol{G}_{\mathbf{RO}}$ gradient consisting of the sum of two physical gradients with variable amplitudes. The direction of each $\boldsymbol{G}_{\mathbf{RO}}$ varies depending on the particular gradient amplitudes.

all echoes will contribute significantly to the image contrast. Any hardware imperfections or patient motion at any point in the scan will produce artifacts.

While radial scanning uses varying G_{RO}, its magnitude is constant during each line. Two-dimensional spiral sampling is a technique where the G_{RO} gradient amplitude varies in magnitude during the echo sampling. Specifically, the two gradients perpendicular to G_{SS} are both varied in a spiral fashion during the echo sampling. This has the result of generating a raw dataset that has data points forming a spiral *k*-space (Figure 5.19). The central points of *k*-space are usually acquired early in the data collection period, as this allows a shorter *TE* to be used. Regridding in both k_x and k_y is necessary to ensure a constant density *k*-space prior to Fourier transformation.

5.9 Phased-array coils

In Chapter 2, the use of a receiver coil in the MR measurement process was described. Receiver coils have many different sizes and shapes, but have one common characteristic: their effective axis (or coil axis) is always normal or perpendicular to $\boldsymbol{B}_0$. For loop coils (consisting of a loop of wire), the effective axis is normal to the direction of the loop. For other coil designs, the effective axis is less obvious, but will always be perpendicular to $\boldsymbol{B}_0$ in all cases.

Another consideration in coil design is the sensitive volume for the coil. For simple loop-type coils, the sensitive volume is roughly equal to one radius in

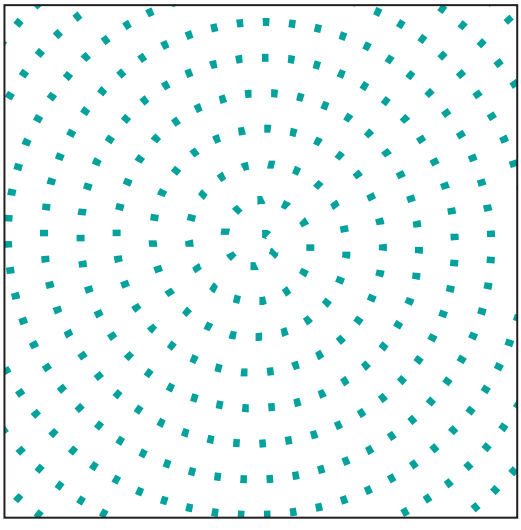

Figure 5.19 Spiral filling of *k*-space, two-dimensional. The signal is sampled with the gradients perpendicular to G_{SS} varying in a spiral fashion.

distance normal to the surface of the coil; in other words, the coil penetration is approximately one radius in distance from the surface of the loop. One type of coil, known as a surface coil, consists of one or more loops. These coils are most sensitive to signals from tissue near the surface of the coil with progressively less signal from tissue farther away from the coil surface. The size of the loop is a significant factor in the coil sensitivity, with larger coils being less sensitive. This is caused by a property known as the coil loading (see Chapter 14), in which the patient coupling or loading of the coil affects the coil sensitivity. It is important that the patient anatomy fill the coil-sensitive volume as much as possible to ensure that the coil operates most efficiently.

For surface coils such as those used for spine imaging, this loss of sensitivity limits the size of the coil that can be used effectively, and the associated anatomical coverage. To overcome this limitation, multiple smaller coils known as phased-array coils have been developed. These coils are arranged in such a manner that they do not interfere with each other (little mutual inductance). Each individual coil in the array is an independent receiver coil that measures the signal from its sensitive area (Figure 5.20). A complete *k*-space is acquired and processed for each coil in the array. The resulting "subimages" are combined to produce an image from a larger anatomical region than is possible for an individual coil, similar to creating a panorama picture by splicing a series of smaller photographs together (Figure 5.21). Phased-array coils are not restricted to posterior positioning as for spine image, but are also used for scanning of anterior anatomy in abdominal or thoracic imaging. Several manufacturers have phased-array coils for examining other regions of the body (for example, head, neck, and knee).

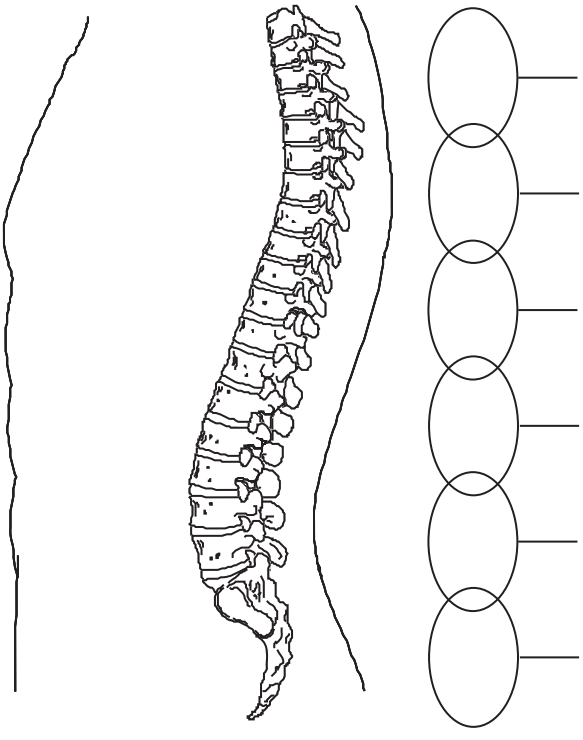

Figure 5.20 Phased-array coils. A large area such as the spine can be scanned using an array of smaller coils. The images from each coil can be combined to form the final image.

5.10 Parallel acquisition methods

In the description of phased-array coils above, each coil of the array is used to acquire a portion of the complete image, with the spatial resolution of each coil subimage equal to that of the final image. While the final image is produced by the combination of the subimages from the individual coils, each coil acquires minimal information away from its sensitive volume in the immediate area of the coil. Another application of phased-array coils uses the unique position of each coil within the array to augment the phase encoding process. This approach is used in so-called parallel acquisition methods. In the presence of G_{PE} in the appropriate direction, each coil experiences a different magnetic field $\boldsymbol{B}_i$ due to its location (equation (4.1)) and the spins that the coil senses will have different resonant frequencies (equation (4.2)). Rather than process the signal from each coil separately, the signals from all coils are merged to produce a single image prior to final processing. The measured signals are combined earlier in the image reconstruction process than with conventional phased-array coil imaging so that subimages from each coil are not representative of the final result; they are only

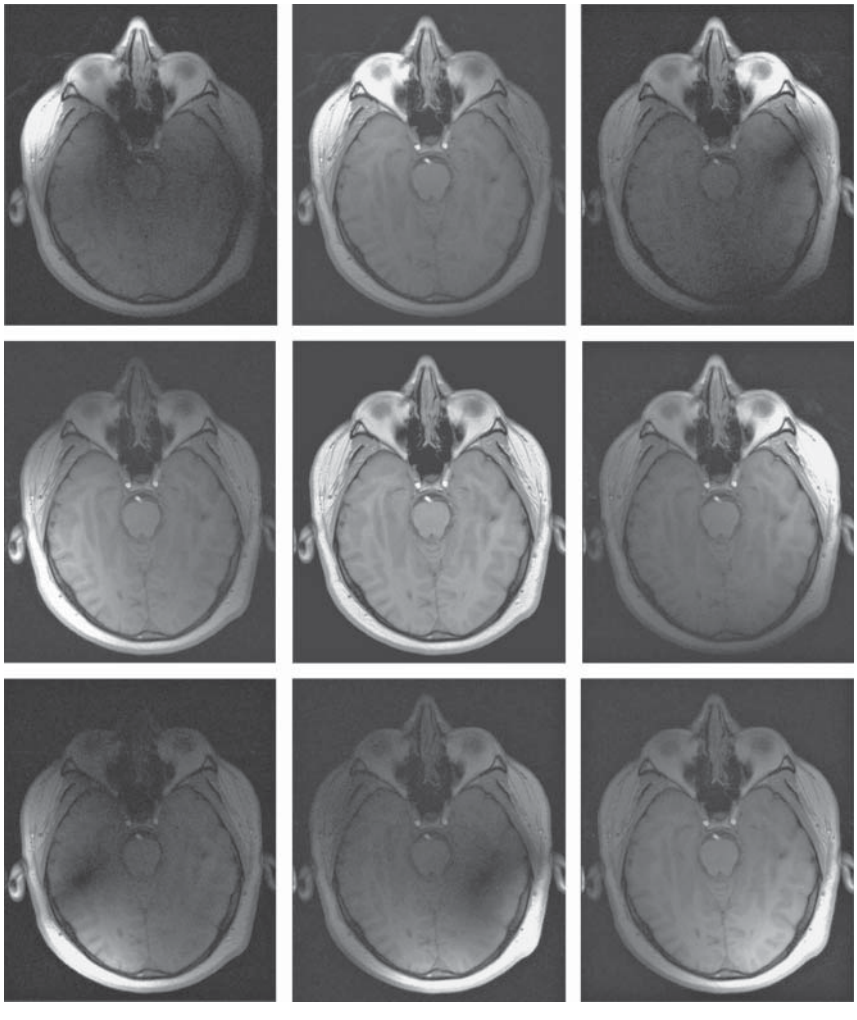

Figure 5.21 Images from the individual coils of an array (outer ring of images) can be combined to produce a single image (central image). Each outer image is sensitive to signals in its vicinity.

suitable when processed with the data from the other coils. This merger of signals enables fewer G_{PE} amplitudes to be used in the scan, so that the scan time can be reduced by a factor up to and including the number of coils used in the process, known as the acceleration factor.

This decrease in scan time is not without a penalty. The SNR is reduced for parallel acquisition techniques compared to the complete scan, with the SNR reduction greater for higher acceleration factors. This SNR reduction is attributed to two factors. The first is the simple fact that, by decreasing the sampling time, the SNR decreases as shown in equation (5.1). This reduced sampling time affects

every voxel, so it leads to a uniform drop in SNR throughout the image. The second cause is known as the g-factor, or geometric factor. In voxels that are close to one coil but far from the other coils, it is relatively easy to "unmerge" the information, but it becomes difficult in voxels that are equidistant from all of the coils. This leads to a spatial variation in SNR where voxels near one of the receive coils will have a higher SNR than voxels that are approximately equidistant from all receive coils.

As a result, parallel acquisition techniques are most appropriate for scan protocols where the SNR is sufficiently high. In these circumstances, the more efficient data collection process can be used to improve the spatial resolution (by increasing N_{PE}), or reduce the scan time.

There are two classes of parallel techniques that are used in clinical scanning, based on when the merger of coil signals is performed: *k*-space-based and image-based (Figure 5.22). The difference between the techniques is the point during the data processing when the signals are combined. Both classes used increased ΔG_{PE} with fewer N_{PE} compared to a complete scan. Both classes are also computationally intensive, placing significant demands on the image reconstruction computer. Regardless of the method, there are four requirements that must be met to ensure that the data collection process does not induce artifacts:

1. Multiple receiver coils must be used. There must be a separate receiver coil at different spatial positions within the magnetic field. Most parallel acquisition techniques use phased-array coils.
2. Each receiver coil must experience a different B_i when G_{PE} is applied. This is easiest accomplished if the G_{PE} direction is parallel to the line connecting the coil centers (Figure 5.23). This is to ensure that each coil contributes different frequency components to the postprocessing. Failure to meet this requirement can potentially cause aliasing artifacts, which may be subtle or severe (see Chapter 9).
3. The FOV in both directions should be large enough so that minimal tissue is excited outside the FOV. While this is not a mandatory requirement, severe artifacts can occur if the FOV is significantly smaller than the anatomical region under observation.
4. The differences in individual coil sensitivities must be eliminated before the signal combination. If one coil is more sensitive than another due to hardware differences, then its contribution will be exaggerated in the final image, potentially causing artifacts. To eliminate this, calibration or reference scans are performed either prior to or during the primary scan that are used to compensate for the manufacturing imperfections.

The *k*-space-based parallel acquisition techniques merge the coil signals prior to Fourier transformation. In normal imaging, these higher harmonics produce aliasing artifacts (see Chapter 9). In the *k*-space-based techniques, the signals measured by the coils are not processed individually but are used to extract the correct (unaliased) signal from the combination signal (Figure 5.24).

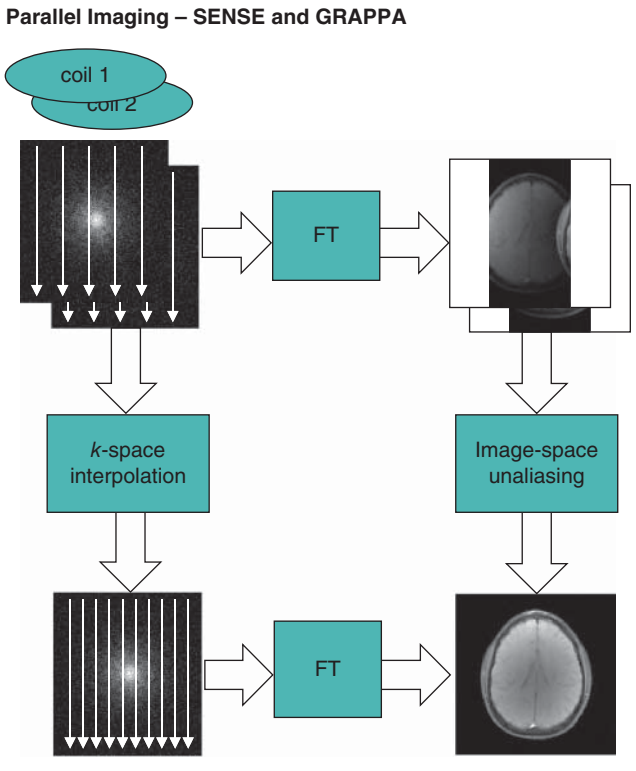

Figure 5.22 Principle of parallel imaging. A raw data set is acquired from each coil element. The data sets have a reduced number of lines, allowing for shorter measurement times. For *k*-space-based methods (solid lines), the raw data sets are combined to form a complete raw data set. The complete raw data set is processed to produce the final image. For image-based methods (dashed lines), the raw data sets are processed to produce images, and the images are combined to form the final image.

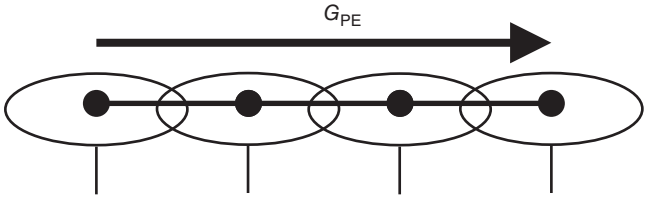

Figure 5.23 The direction of $\boldsymbol{G_{PE}}$ should be aligned with the coil geometry axis. The different position of each coil means that the magnetic field will differ at each location.

Each element of the array will detect different amplitudes of the harmonics that are produced by a particular k_y line due to its different location. The coil geometry is such that sinusoidal patterns can be generated mathematically using linear combinations of the coil sensitivities, properly resolving the harmonics. Two *k*-space-based techniques are commonly used: SMASH (Simultaneous

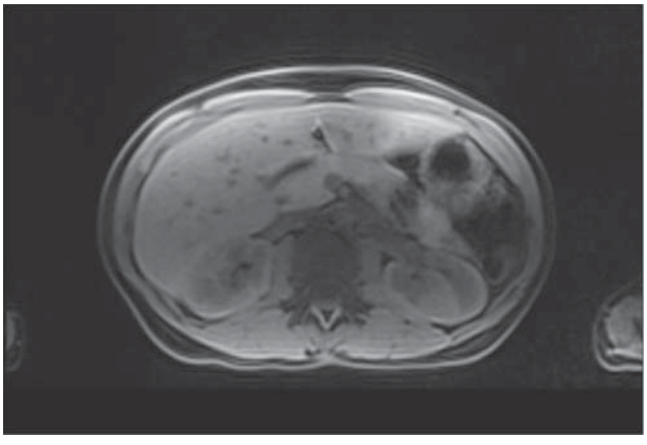

Figure 5.24 Three-dimensional transverse *T1*-weighted spoiled gradient echo image of abdomen with fat suppression, acquired using a 32-channel body array receiver coil. Scan parameters: GRAPPA with acceleration factors of 2 each in both k_y and k_z directions; *TR*, 4.9 ms; *TE*, 2.4 ms; excitation angle, 10°; acquisition matrix, N_{PE}, 131 and N_{RO}, 256 with twofold readout oversampling; FOV, 262 mm PE × 350 mm RO; effective slice thickness, 3.5 mm; time of acquisition, 8 s.

Acquisition of Spatial Harmonics) and GRAPPA (Generalized Autocalibrating Partially Parallel Acquisitions). The primary difference between them is when the calibration scans are acquired. SMASH acquires the calibration scans as a separate scan, enabling the primary scan time reduction to be directly proportional to the number of coils parallel to G_{PE}. The calibration scans can be used in multiple scans as long as the same coils are used. GRAPPA acquires the calibration scans as part of the primary scan. While this approach reduces the scan time savings, the calibration scans can be used in the final image as well, improving the SNR.

The other class of parallel acquisition techniques is image-based. The primary example of this approach is SENSE (Sensitivity Encoding). With SENSE, the number of k_y lines is reduced but Δk_y is increased so that the total span of *k*-space is maintained, effectively reducing FOV_{PH} for the image. An image is produced from the *k*-space sampled from each coil that contains both the correct image and the aliased portion due to the higher harmonics, but the amount of wrap at each spatial location is different for each coil. By comparing the different images and knowing the coil position and sensitivity, an unaliased image can be extracted from the different partial images.